

Low Carrier Density Epitaxial Graphene Devices On SiC

Yanfei Yang,* Lung-I. Huang, Yasuhiro Fukuyama, Fan-Hung Liu, Mariano A. Real, Paola Barbara, Chi-Te Liang, David B. Newell, and Randolph E. Elmquist

Graphene, the first genuinely two-dimensional material,^[1] is a single layer of carbon forming a simple hexagonal lattice. Remarkable electrical properties such as high mobility and an anomalous quantum Hall effect (QHE) were demonstrated in exfoliated graphene flakes and attracted enormous interest for many practical applications.^[2–5] However, mechanical exfoliation of graphite cannot provide graphene suitable for commercial wafer-size electronics or precise resistance metrology due to the size limitation of the exfoliated graphene flakes (usually up to tens of micrometers).

When SiC substrates are annealed at temperatures above 1000 °C in ultra-high vacuum or an inert gas atmosphere, carbon remains on the SiC surface after Si sublimation and rearranges to form graphene layers. This epitaxial graphene (EG) is ready for large-scale device fabrication without transfer to another insulating substrate. Graphene grown on the silicon-terminated face (Si-face) of hexagonal SiC wafers can form large domains due to registry with the azimuthal orientation of the SiC crystal. On the Si-face, EG also has more controllable growth kinetics, compared to the graphene grown on the opposite (carbon) face.

Recently, growth of homogeneous monolayer EG on the Si-face of SiC has been improved by optimizing the

annealing temperature and background gas conditions.^[6–10] QHE plateaus have been observed in various magneto-transport measurements and the robust quantized Hall resistance (QHR) plateau with filling factor $\nu = 4(i + 1/2) = 2$, where $i = 0$ is the lowest Landau level (LL) index for monolayer graphene, has been shown to be equivalent to that of conventional 2D electron systems based on semiconductor heterostructures at low temperature (<4 K), which are the basis of present-day electrical resistance metrology.^[11–18] Since monolayer graphene's anomalous LL energy spacing is quite large compared to the spacing of LLs in semiconductor heterostructures, graphene QHR standards could well be used at higher temperatures or lower magnetic field strengths than today's GaAs/AlGaAs devices.^[19] However, for use at reasonable magnetic field levels, QHR devices must have carrier densities $n \leq 10^{12} \text{ cm}^{-2}$. The accepted best practices for precise QHR measurements also specify vanishing channel longitudinal resistivity with low, Ohmic contact resistance values.^[20] So far, only a few EG devices exist that display all of these qualities.

Strong electron (n-type) doping is imparted to Si-face EG by a buffer layer that is covalently bonded to the SiC substrate. Fermi energies determined by in situ angle-resolved photo-emission spectroscopy (ARPES) confirm that an intrinsic n-type doping near 10^{13} cm^{-2} exists in as-grown EG.^[16,21,22] Various techniques such as gating and chemical doping have been developed to compensate intrinsic doping levels.^[11,12,15,16,23]

Here we report high mobility and low carrier density in un-gated EG devices that are produced with high yield when a metal protective layer is deposited directly on as-grown EG. This layer prevents EG contact with most organic residues (see **Figure 1**). When diluted aqua regia (DAR) is used as the final etching agent in this process, most of our Hall bar devices based on Si-face EG have carrier densities in the range of $3 \times 10^{10} \text{ cm}^{-2}$ to $3 \times 10^{11} \text{ cm}^{-2}$, much lower than those obtained by conventional lithography. Well-defined $\nu = 2$ plateaus are observed in moderate magnetic fields, and the doping level can be controlled by heat treatment.

Five samples diced from semi-insulating 4H- or 6H-SiC(0001) wafers were annealed at 1900 °C or 1950 °C in an Ar background at 101–105 kPa using a controlled Si sublimation process (see supporting information).^[8] Raman microscopy shows that homogeneous graphene covers 95% of the central sample area for samples prepared by the same methods and under similar conditions. In the critical new processing step, a metal bilayer (5 nm Pd + 10 nm Au, for

Dr. Y. Yang, L.-I. Huang, Dr. D. B. Newell,

Dr. R. E. Elmquist

National Institute of Standards and Technology (NIST)

Gaithersburg, MD 20899–8171

E-mail: yanfei.yang@nist.gov

Dr. Y. Yang, Prof. P. Barbara

Department of Physics

Georgetown University

Washington, DC 20057–1228

L.-I. Huang, Prof. C.-T. Liang

Department of Physics

National Taiwan University

Taipei 10617, Taiwan

Dr. Y. Fukuyama

National Metrology Institute of Japan (NMIJ)/AIST

Tsukuba, Ibaraki 305–8563, Japan

F.-H. Liu, Prof. C.-T. Liang

Graduate Institute of Applied Physics

National Taiwan University

Taipei 10617, Taiwan

M. A. Real

Instituto Nacional de Tecnologia Industrial

San Martin, Buenos, Aires B1650WAB, Argentina



DOI: 10.1002/sml.201400989

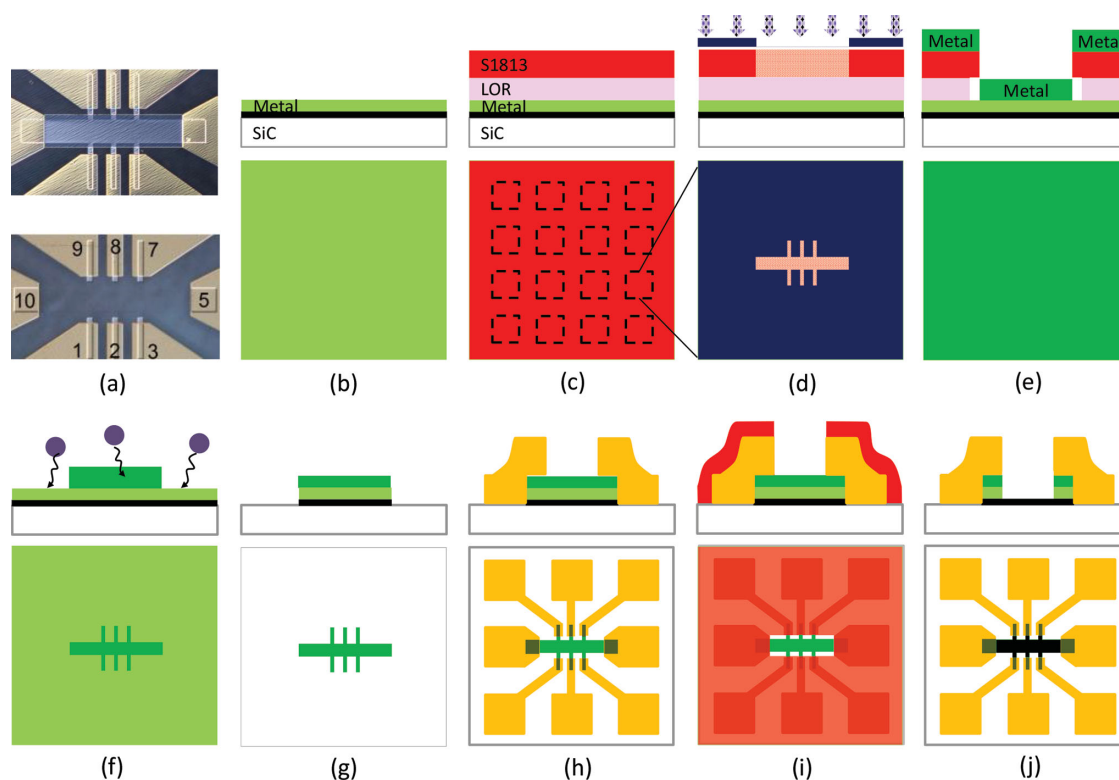


Figure 1. Device images and fabrication process. a) Optical images (upper) with metal protective layer covering the Hall bar area ($600\ \mu\text{m} \times 100\ \mu\text{m}$) of a device and (lower) after removing the metal layer. Six $20\ \mu\text{m}$ wide voltage probes (1,2,3,7,8,9) are located in the central $200\ \mu\text{m}$ wide region of the Hall bar, with $100\ \mu\text{m}$ longitudinal spacing. Source and drain are labeled 5 and 10. b) Metal is first evaporated on as-grown graphene. c) Spin-coating of bi-layer photoresist. Each dashed square indicates a single device area. d) UV-exposure (with enlarged single device area shown). e) Undercut profile is formed to assist the lift-off after evaporation of a second metal layer (green). f) Ar reactive-ion-etching is applied. g) Metal-protected EG Hall bar after RIE. (h) Protected graphene Hall bar with contact electrodes. i) An etching window is opened in Hall bar area. j) Metal over Hall bar area is etched by DAR, followed by optional stripping of photoresist using acetone.

samples S1–S3) or a single 30-nm-thick Au layer (for S4 and S5) was deposited directly on the as-grown EG surface after a 10 min, $115\ ^\circ\text{C}$ dehydration baking (Figure 1b). This protective metal layer prevented the intermediate processing steps from contaminating the graphene and was removed from the Hall bars using diluted aqua regia (DAR) in the final step of fabrication (Figure 1j).

Each sample has 16 similar Hall-bar devices (Figure 1c). Devices having eight Ohmic contacts and sheet resistance R_s lower than $21\ \text{k}\Omega$ (see **Table 1**) were selected for low-temperature magneto-transport characterization. Here, R_s is the average four-terminal resistance scaled by the width-to-length ratio of the channel $R_s = \frac{(R_{13} + R_{79})}{2} \frac{w}{L}$, where L is the spacing between voltage probes, w is the channel width, R_{13} and R_{79} are four-terminal resistance measured across contacts 1–3 and 7–9 (Figure 1a), respectively. All cryogenic measurements were made in a liquid-helium cryostat using a 9 T superconducting magnet. The device carrier density and mobility values determined at $T < 4.5\ \text{K}$ using low-field magneto-transport are listed in Table 1, as well as the wafer properties, the maximum annealing temperature and the annealing time at that temperature. Devices on four of the samples showed homogeneous carrier densities n that are lower than $3.2 \times 10^{11}\ \text{cm}^{-2}$.

We focus first on magneto-transport measurements of device S4D4. **Figure 2a** shows that the carrier density

and mobility at $4.3\ \text{K}$ are $n = 2.4 \times 10^{11}\ \text{cm}^{-2}$ and $\mu = 5200\ \text{cm}^2\ \text{V}^{-1}\ \text{s}^{-1}$, respectively. Prominent Shubnikov-de Haas (ShdH) oscillations are present with minima at the $\nu = 6$ and $\nu = 10$ filling factors, indicating good homogeneity along the device channel. Precise dc measurements at $1.6\ \text{K}$ using a cryogenic current comparator bridge at a source-drain current of $40\ \mu\text{A}$ show that the device is nearly fully quantized with a longitudinal resistivity of $\rho_{xx} = 0.05 \pm 0.01\ \Omega$ and a QHR at the $\nu = 2$ plateau of $R_{xy} = (h/2e^2) \times (1 - 4 \times 10^{-6} \pm 2 \times 10^{-6})$.^[24] Very nearly the same electronic characteristics and level of QHR quantization were measured for both magnetic field directions, with six of eight contacts of device S4D4 having contact resistance below $4\ \Omega$. Contact resistance values of S1D2 and S4D4 were measured at the highest available field strength ($\pm 9\ \text{T}$) in the quantized Hall plateau region using three-terminal measurements. Low Ohmic contact resistances were observed for devices in both of these two samples, subject to variability in longitudinal resistance in the side contact channels.

A significant drop in n-type carrier density over time was observed during the first month after fabrication in devices S1D1 and S1D2. These samples were stored under ambient laboratory conditions ($23\ ^\circ\text{C}$, 40% relative humidity) when not in use. Figure 2b shows two sets of data at $T = 4.3\ \text{K}$ with ρ_{xx} and R_{xy} measured in S1D2 using lock-in amplifiers. In the data recorded one week after the fabrication (dashed

Table 1. Growth conditions and transport characteristics for five samples approximately one month after fabrication, from low-current ac measurements recorded with lock-in amplifiers; Samples S1, S2, and S3 were diced from the same 6H-SiC wafer. Samples S1 and S2 were annealed and processed together, and thus are grouped together. The carrier density and mobility were measured at 4.0 K to 4.5 K for samples S1 through S4, and at 1.6 K for sample S5. Standard deviations of the carrier densities for each sample group are low, ranging from $0.5 \times 10^{11} \text{ cm}^{-2}$ to $0.8 \times 10^{11} \text{ cm}^{-2}$.

Device name	Wafer type	Growth Conditions [°C min ⁻¹]	Electron density n [cm ⁻²]	Mobility μ [cm ² V ⁻¹ s ⁻¹]	R_s [k Ω] $B = 0$
S1D1	6H-SiC	1900/30	1.3×10^{11}	11 000	4.4
S1D2			1.4×10^{11}	6500	7.1
S1D3			5.1×10^{10}	10 200	11.9
S2D1	6H-SiC	1900/30	4.2×10^{10}	7400	20.2
S3D1			-5.4×10^{10}	7900	14.6
S3D2	4H-SiC	1900/18	5.1×10^{10}	10 800	11.3
S3D3			4.0×10^{10}	8600	18.2
S3D4			7.0×10^{10}	4400	20.6
S3D5			6.4×10^{10}	8500	11.4
S4D1			2.0×10^{11}	3600	4.6
S4D2	1.9×10^{11}	6000	5.5		
S4D3	3.1×10^{11}	2600	7.8		
S4D4	2.4×10^{11}	5200	5.1		
S4D5	3.2×10^{11}	2100	9.0		
S5D1	4H-SiC	1950/15	8.0×10^{11}	2500	3.1
S5D2			7.4×10^{11}	2200	3.8
S5D3			8.2×10^{11}	2000	3.8
S5D4			8.2×10^{11}	1640	4.6
S5D5			6.3×10^{11}	2200	4.5

lines), a well-developed $\nu = 2$ plateau is present for $B \geq 3.8$ T and the longitudinal resistivity is below 10Ω in the high magnetic field range. In the low magnetic field region, ShdH oscillations are weak. These characteristics may indicate an inhomogeneous carrier concentration along the Hall bar. The solid lines in Figure 2b were measured for device S1D2 one month after device fabrication. The ρ_{xx} profile is compressed and the ShdH oscillations are completely absent. We observe the onset of the $\nu = 2$ Hall plateau at low fields, with $n = 1.3 \times 10^{11} \text{ cm}^{-2}$ and $\mu = 11\,000 \text{ cm}^2 \text{ V}^{-1} \text{ s}^{-1}$. The minimum longitudinal resistivity at high field has approximately doubled to 20Ω .

Over a similar one-month time interval very low carrier concentrations were maintained on sample S3. Some devices that were slightly p-doped soon after fabrication became slightly n-doped. Only device S3D1 remained p-doped after one month in ambient conditions (see Table 1). In all of the devices on sample S3 and some devices on S1 and S2 the Fermi energy is quite close to the Dirac point. Regions dominated by electrons or holes (as puddles) are known to exist in this regime for pristine exfoliated graphene. Although readily apparent $\nu = 2$ Hall plateaus are observed at very low magnetic fields in our devices on sample S3, the transport results show that the devices with the lowest carrier density are not well-quantized at any magnetic field level, with minimum $\rho_{xx} > 300 \Omega$ and $R_{xy} \approx h/2e^2$. The effect of very low carrier concentration on transport properties in graphene close to the Dirac point is not the main issue of this paper and will be reported elsewhere. One could speculate that adsorption

on the graphene surface may be dominated by van der Waals attraction between the graphene and the adsorbed molecules, leading to a preferred equilibrium level of adsorption for a particular molecular dopant on clean epitaxial graphene. However, chemical and/or physical attachment mechanisms that are independent of the carrier density are also possible.

Our post-processing studies show that the variation in the carrier density with time is very likely due to molecular doping, with gradual desorption of the doping molecules deposited by aqua regia and adsorption of other molecules from the air. Atomic force microscope (AFM) images taken after fabrication show indications of foreign matter at a very small length scale that were not present prior to device fabrication, suggesting that the EG surface may be covered with molecular adsorbates (see Figure S1, Supporting Information).

We subjected sample S4 to heat-treating (HT) in Ar gas (99.999%) at relatively low temperatures, alternating with 1 s immersion in DAR (followed immediately by rinsing in deionized water). After each step, transport measurements were made. **Table 2** shows the results of magneto-transport measurements on S4D4 at temperatures near 4.5 K. The n-type doping levels were raised by more than an order of magnitude when the sample was heat-treated at temperatures of $250 \text{ }^\circ\text{C}$ and $175 \text{ }^\circ\text{C}$, and very low n-type carrier concentrations were restored by dipping the sample in DAR. When the sample was stored for six days in ambient air after HT at $175 \text{ }^\circ\text{C}$, the n-type carrier concentration decreased by 63%, but no change was observed when the sample was stored

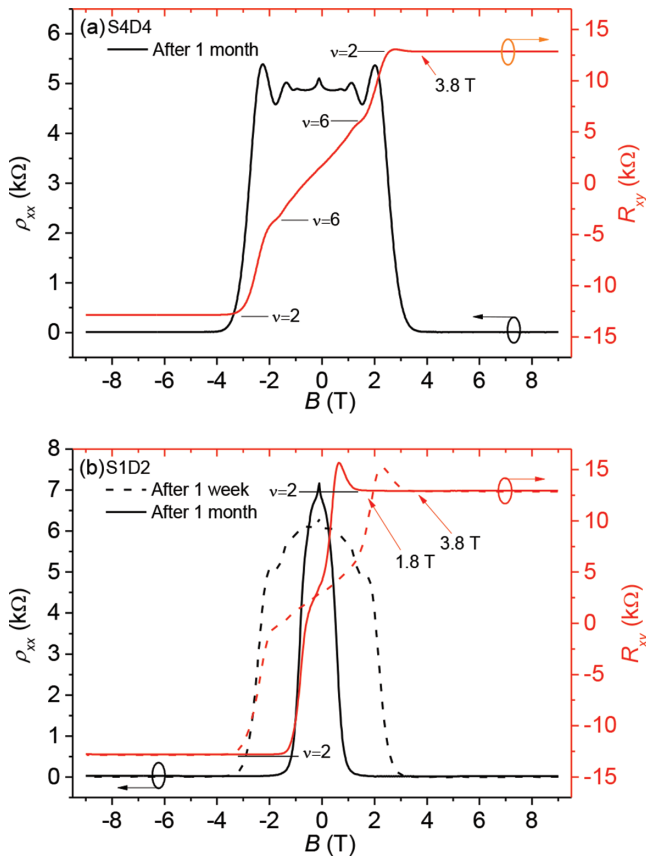


Figure 2. a) Longitudinal resistivity (black) and Hall resistance (red) of device S4D4 at 4.3 K, one month after fabrication. b) Similar measurements for device S1D2 at 4.3 K measured one week (dashed lines) and one month (solid lines) after the fabrication, respectively.

for four days in He gas at cryogenic temperatures following the HT at 250 °C. The device magneto-transport characteristics were not obviously degraded by DAR/HT cycling, and extremely well-developed QHR plateaus were observed after the final processing step shown in Table 2.

We conclude with results of processing sample S5 with Polymethyl methacrylate (PMMA), a common electron-beam photoresist. The possible applications of this type of polymer would be for stabilizing the carrier concentration, photochemical gating, or to create p-n junctions.^[23,25,26]

Table 2. Results of post-processing of device S4D4, measured at $4.54 \text{ K} \pm 0.04 \text{ K}$. DAR results in strongly reduced n-type doping, while heat treatment increases the n-type carrier concentration.

Device S4D4 Process, T (time)	Electron density n [cm^{-2}]	Mobility μ [$\text{cm}^2 \text{V}^{-1} \text{s}^{-1}$]	R_s [$\text{k}\Omega$] $B = 0$
Initial fabrication	2.4×10^{11}	5200	5.1
HT, 250 °C (2.5 h)	2.9×10^{12}	2030	1.0
Helium, <30 K (100 h)	2.9×10^{12}	2030	1.0
DAR, 20 °C (1 s)	4.0×10^{10}	16 800	10.3
HT, 175 °C (2.5 h)	1.8×10^{12}	2800	1.3
Ambient air (140 h)	6.8×10^{11}	6100	1.5
DAR, 20 °C (1 s)	-5.0×10^{10}	10 200	12.1
HT 100 °C (0.5 h.)	2.9×10^{11}	5160	4.2

Figure 3a shows transport characteristics of device S5D2 before applying PMMA, with n-type carrier density of $7.4 \times 10^{11} \text{ cm}^{-2}$. Pronounced ShdH oscillations corresponding to filling factor indices $\nu = 2, 6, 10,$ and 14 are clearly observed with the well-developed $\nu = 6$ plateau occurring for R_{xy} between 4 T and 6 T. **Figure 3b** shows results after the sample was coated with a PMMA layer and cured; the carrier density increased to $n = 2.5 \times 10^{12} \text{ cm}^{-2}$. Finally, the polymer layer on S5 was removed, and the results in **Figure 3c** show that the carrier density once again increased to $5.7 \times 10^{12} \text{ cm}^{-2}$. Increasing carrier density may be due to displacement or removal of the p-type doping agent from the EG surface and polymer residue (see **Figure S2**, Supporting Information).^[27] On the other hand, the deterioration of the mobility, along with the broadened weak localization peak indicate the increase of disorder in the Hall bar area. This is consistent with the decrease of the simulated phase coherence length l_ϕ

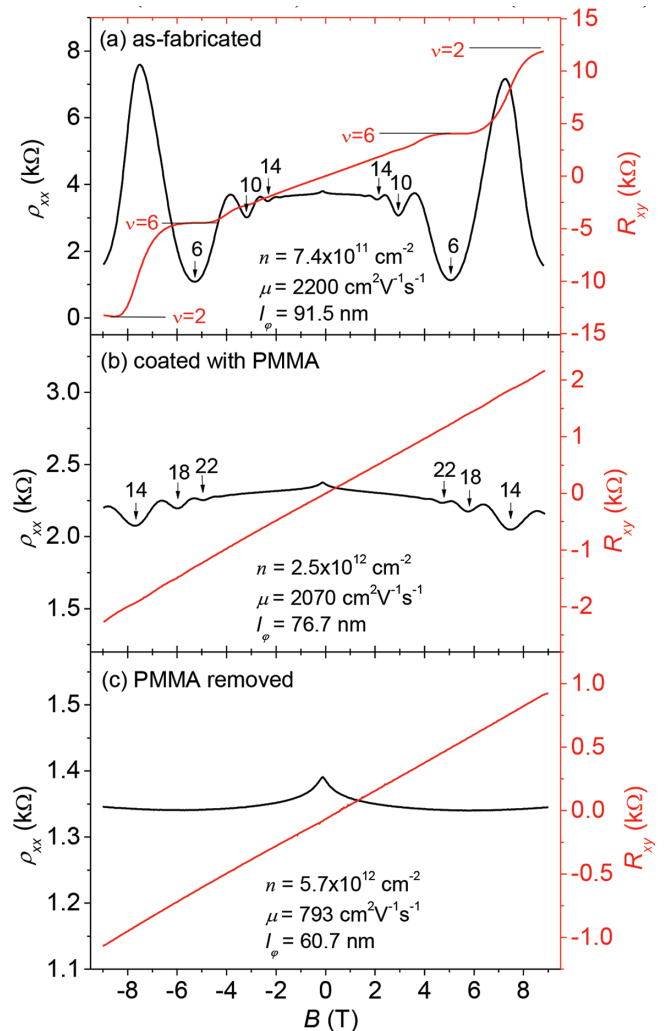


Figure 3. Magneto-transport results (ρ_{xx} and R_{xy}) for device S5D2 at 1.5 K (note changes in scale for the vertical axes): a) as fabricated with the 30-nm-thick Au layer etched by aqua regia; b) after spin-coating using PMMA and curing; c) after removal of PMMA. Landau filling factors are used to identify some features. Insets: carrier density n , mobility μ and phase coherence length l_ϕ extracted by fitting the weak localization peak at low field.

(insets of Figure 3), which is simulated by fitting the low-field conductivities to the weak localization model:^[28]

$$\delta\sigma_{xx}^{WL} = G_0 \left\{ \psi \left(\frac{1}{2} + \frac{B_\phi}{B} \right) - \psi \left(\frac{1}{2} + \frac{B_{tr}}{B} \right) + \ln \left(\frac{B_{tr}}{B_\phi} \right) \right\},$$

where ψ is the digamma function, $G_0 = e^2/(\pi h)$, the transport magnetic field $B_{tr} = \hbar/(2el^2)$, and $B_\phi = \hbar/(4el_\phi^2)$. We found that l_ϕ is 91.5 nm, 76.7 nm and 60.7 nm for data shown in Figure 3a–c, respectively.

Our new protective precious-metal masking process for fabrication of graphene-based devices results in very low carrier concentrations and high mobility. Elsewhere, enhanced p-type doping in EG has been produced by gold adatoms but only after post-annealing to at least 700 °C.^[29] Intercalation of hydrogen, gold, oxygen and other atoms beneath the EG buffer layer also can produce a p-type carrier concentration,^[16] but these processes only occur at high temperatures. The temperatures encountered in our fabrication are never higher than 180 °C. Energy-dispersive X-ray spectroscopy (EDS) spectra showed only carbon, silicon, and trace atomic concentrations of oxygen. No indication of either Au or Pd was found on the aqua-regia-exposed EG regions. Thus, we believe that our results unequivocally show that extrinsic molecular doping is responsible for the low carrier concentration, and this doping process is initiated by aqua regia.

Both of the components of aqua regia, nitric acid and hydrochloric acid, are potent p-doping agents of graphene.^[30,31] Since oxygen is the only significant component in the EDS spectra from as-fabricated graphene devices other than carbon and silicon, evidence points to HNO₃ as the primary doping agent, either by itself or by some chemical process in concert with other molecules present in the air. The observed changes in the level of carrier activity after exposure to the ambient air support the notion of additional doping processes.

In summary, we have fabricated devices without polymer residues using epitaxial graphene and found that the carrier density is typically below $3 \times 10^{11} \text{ cm}^{-2}$ and is uniform on the same sample to within $1 \times 10^{11} \text{ cm}^{-2}$ after molecular doping by DAR. On sample S4 we observed highly quantized $\nu = 2$ QHR plateaus with $R_{xy} \approx h/(2e^2)$ and near-zero longitudinal resistivity. Device S4D4 displays almost fully-quantized Hall plateaus, showing that EG is not significantly damaged by the deposition of precious metals (Pd, Au) or by diluted aqua regia, even after several immersion steps.

This new fabrication and doping process avoids organic contamination of devices based on epitaxial graphene grown on SiC. The method thus provides an alternate route for producing large-scale, highly ordered, low carrier-density epitaxial graphene for QHR standards and for the study of low-carrier density graphene.

Supporting Information

Supporting Information is available from the Wiley Online Library or from the author.

Acknowledgements

The authors gratefully acknowledge support for Y. Yang's work at NIST, federal grant #70NANB12H185.

- [1] K. S. Novoselov, A. K. Geim, S. V. Morozov, D. Jiang, Y. Zhang, S. V. Dubonos, I. V. Grigorieva, A. A. Firsov, *Science* **2004**, *306*, 666.
- [2] A. H. Castro-Neto, F. Guinea, N. M. R. Peres, K. S. Novoselov, A. K. Geim, *Rev. Mod. Phys.* **2010**, *81*, 109.
- [3] K. I. Bolotin, K. J. Sikes, Z. Jiang, M. Klima, G. Fudenberg, J. Hone, P. Kim, H. L. Stormer, *Solid State Commun.* **2008**, *146*, 351.
- [4] K. S. Novoselov, A. K. Geim, S. V. Morozov, D. Jiang, M. I. Katsnelson, I. V. Grigorieva, S. V. Dubonos, A. A. Firsov, *Nature* **2005**, *438*, 197.
- [5] Y. Zhang, Y.-W. Tan, H. L. Stormer, P. Kim, *Nature* **2005**, *438*, 201.
- [6] C. Virojanadara, M. Syväjärvi, R. Yakimova, L. I. Johansson, A. A. Zakharov, T. Balasubramanian, *Phys. Rev. B* **2008**, *78*, 245403.
- [7] K. V. Emtsev, A. Bostwick, K. Horn, J. Jobst, G. L. Kellogg, L. Ley, J. L. McChesney, T. Ohta, S. A. Reshanov, J. Röhrl, E. Rotenberg, A. K. Schmid, D. Waldmann, H. B. Weber, T. Seyller, *Nat. Mater.* **2009**, *8*, 203.
- [8] M. A. Real, E. A. Lass, F.-H. Liu, T. Shen, G. R. Jones, J. A. Soons, D. B. Newell, A. V. Davydov, R. E. Elmquist, *IEEE Trans. Instrum. Meas.* **2013**, *62*, 1454.
- [9] C. Berger, Z. Song, X. Li, X. Wu, N. Brown, C. Naud, D. Mayou, T. Li, J. Hass, A. N. Marchenkov, E. H. Conrad, P. N. First, W. A. de Heer, *Science* **2006**, *312*, 1191.
- [10] L. O. Nyakiti, R. L. Myers-Ward, V. D. Wheeler, E. A. Imhoff, F. J. Bezares, H. Chun, J. D. Caldwell, A. L. Friedman, B. R. Matis, J. W. Baldwin, P. M. Campbell, J. C. Culbertson, C. R. Eddy Jr., G. G. Jernigan, D. K. Gaskill, *Nano Lett.* **2012**, *12*, 1749.
- [11] T. Shen, J. J. Gu, M. Xu, Y. Q. Wu, M. L. Bolen, M. A. Capano, L. W. Engel, P. D. Ye, *Appl. Phys. Lett.* **2009**, *95*, 172105.
- [12] J. Jobst, D. Waldmann, F. Speck, R. Hirner, D. K. Maude, T. Seyller, H. B. Weber, *Phys. Rev. B* **2010**, *81*, 195434.
- [13] A. Tzalenchuk, S. Lara-Avila, A. Kalaboukhov, S. Paolillo, M. Syväjärvi, R. Yakimova, O. Kazakova, T. J. B. M. Janssen, V. Fal'ko, S. Kubatkin, *Nat. Nanotechnol.* **2010**, *5*, 186.
- [14] W. Pan, S. W. Howell, A. J. Ross III, T. Ohta, T. A. Friedmann, *Appl. Phys. Lett.* **2010**, *97*, 252101.
- [15] S. Tanabe, Y. Sekine, H. Kageshima, M. Nagase, H. Hibino, *Appl. Phys. Exp.* **2010**, *3*, 075102.
- [16] E. Pallecchi, M. Ridene, D. Kazazis, C. Mathieu, F. Schopfer, W. Poirier, D. Mailly, A. Ouerghi, *Appl. Phys. Lett.* **2012**, *100*, 253109.
- [17] A. Satrapinski, S. Novikov, N. Lebedeva, *Appl. Phys. Lett.* **2013**, *100*, 173509.
- [18] T. J. B. M. Janssen, A. Tzalenchuk, R. Yakimova, S. Kubatkin, S. Lara-Avila, S. Kopylov, V. I. Fal'ko, *Phys. Rev. B* **2011**, *83*, 233402.
- [19] T. J. B. M. Janssen, J. M. Williams, N. E. Fletcher, R. Goebel, A. Tzalenchuk, R. Yakimova, S. Lara-Avila, S. Kubatkin, V. I. Fal'ko, *Metrologia* **2012**, *49*, 294.
- [20] F. Delahaye, B. Jeckelmann, *Metrologia* **2003**, *40*, 217.
- [21] S. Y. Zhou, D. A. Siegel, A. V. Fedorov, A. Lanzara, *Phys. Rev. Lett.* **2008**, *101*, 086402.
- [22] C. Riedl, C. Coletti, U. Starke, *J. Phys. D: Appl. Phys.* **2010**, *43*, 374009.
- [23] S. Lara-Avila, K. Moth-Poulsen, R. Yakimova, T. Bjørnholm, V. Fal'ko, A. Tzalenchuk, S. Kubatkin, *Adv. Mater.* **2011**, *23*, 878.
- [24] F. L. Hernandez-Marquez, M. E. Bierzychudek, G. R. Jones Jr., R. E. Elmquist, *Rev. Sci. Instrum.* **2014**, *85*, 044701.

- [25] H.-C. Cheng, R.-J. Shiue, C.-C. Tsai, W.-H. Wang, Y.-T. Chen, *Am. Chem. Soc. Nano* **2011**, *5*, 2051.
- [26] T. Lohmann, K. von Klitzing, J. H. Smet, *Nano Lett.* **2009**, *9*, 1973.
- [27] O. Kazakova, V. Panchal, T. L. Burnett, *Crystals* **2013**, *3*, 191.
- [28] S. Hikami, A. I. Larkin, Y. Nagaoka, *Prog. Theor. Phys.* **1980**, *63*, 707.
- [29] I. Gierz, C. Riedl, U. Starke, C. R. Ast, K. Kern, *Nano Lett.* **2008**, *8*, 4603.
- [30] T. O. Wehling, K. S. Novoselov, S. V. Morozov, E. E. Vdovin, M. I. Katsnelson, A. K. Geim, A. I. Lichtenstein, *Nano Lett.* **2008**, *8*, 173.
- [31] S. Bae, H. Kim, Y. Lee, X. Xu, J.-S. Park, Y. Zheng, J. Balakrishnan, T. Lei, H. R. Kim, Y. I. Song, Y.-J. Kim, K. S. Kim, B. Özyilmaz, J.-H. Ahn, B. H. Hong, S. Iijima, *Nat. Nanotechnol.* **2010**, *5*, 574.

Received: April 10, 2014

Revised: June 16, 2014

Published online: